



**HAL**  
open science

# Mutual approximations between the five main moons of Uranus

S Santos-Filho, M Assafin, B Morgado, R Vieira-Martins, J Camargo, A  
Gomes-Júnior, G Benedetti-Rossi

► **To cite this version:**

S Santos-Filho, M Assafin, B Morgado, R Vieira-Martins, J Camargo, et al.. Mutual approximations between the five main moons of Uranus. *Monthly Notices of the Royal Astronomical Society*, 2019, 490 (3), pp.3464-3475. 10.1093/mnras/stz2841 . hal-03118306

**HAL Id: hal-03118306**

**<https://hal.science/hal-03118306>**

Submitted on 22 Jan 2021

**HAL** is a multi-disciplinary open access archive for the deposit and dissemination of scientific research documents, whether they are published or not. The documents may come from teaching and research institutions in France or abroad, or from public or private research centers.

L'archive ouverte pluridisciplinaire **HAL**, est destinée au dépôt et à la diffusion de documents scientifiques de niveau recherche, publiés ou non, émanant des établissements d'enseignement et de recherche français ou étrangers, des laboratoires publics ou privés.

# Mutual approximations between the five main moons of Uranus

S. Santos-Filho,<sup>1</sup> M. Assafin,<sup>1,3</sup>★ B. E. Morgado<sup>1b,2,3</sup>, R. Vieira-Martins,<sup>1,2,3</sup>  
J. I. B. Camargo,<sup>2,3</sup> A. R. Gomes-Júnior<sup>1b,3,4</sup> and G. Benedetti-Rossi<sup>1b,2,3,5</sup>

<sup>1</sup>Observatório do Valongo/UFRJ, Ladeira do Pedro Antonio 43, Rio de Janeiro, RJ 20080-090, Brazil

<sup>2</sup>Observatório Nacional/MCTI, R. General José Cristino 77, Rio de Janeiro, RJ 20921-400, Brazil

<sup>3</sup>Laboratório Interinstitucional de e-Astronomia - LIneA, Rua Gal. José Cristino 77, Rio de Janeiro, RJ 20921-400, Brazil

<sup>4</sup>UNESP - São Paulo State University, Grupo de Dinâmica Orbital e Planetologia, CEP 12516-410, Guaratinguetá, SP 12516-410, Brazil

<sup>5</sup>LESIA, Observatoire de Paris - Section Meudon, 5 Place Jules Janssen - 92195 Meudon Cedex

Accepted 2019 October 7. Received 2019 September 20; in original form 2019 July 22

## ABSTRACT

Doing high-precision astrometry on Uranus' moons is currently quite challenging. No probes will orbit the system before 2040. New high-precision mutual phenomena measurements will only occur in 2050. Besides, Uranus is slowly passing through a sky region without many stars, which makes it difficult to map field of view (FOV) distortions below 50 mas. In this context, the new astrometric technique of mutual approximations comes in handy. It measures central instants at the closest approach between two moving satellites in the sky plane. Measurements are made on small portions of the FOV, benefiting from the so-called *precision premium*. Approximations and mutual phenomena share geometric principles and parameters, with similar precision in the central instant as indicated by first applications to the Jovian moons. However, mutual phenomena can only be observed at the planet's equinoxes, while approximations always occur. Central instants do not depend on reference stars and are useful in orbit and ephemeris fittings. Here, we present results for 23 mutual approximations between the five main Uranus satellites observed in Brazil during 2015–2018 with a 1.6 m aperture telescope. Digital coronagraphy mitigated Uranus' scattered light, improving measurements for Miranda, Ariel and Umbriel. We measured the impact parameter and relative velocity in milliarcseconds for the first time by using a variant of the method. Relative position errors, including Miranda, were 45 mas per coordinate, twice as good as in classical CCD astrometry for this satellite, and comparable to mutual phenomena. This shows the potential of mutual approximations for improving the current orbits and ephemerides of Uranus' moons.

**Key words:** methods: data analysis – astrometry – ephemerides – planets and satellites: individual: Miranda, Ariel, Umbriel, Titania, Oberon.

## 1 INTRODUCTION

Astrometry of the natural satellites of planets allows for the improvement of the dynamic models of their orbits (Jacobson 2014), which in turn enriches the study of the origin (Charnoz et al. 2011; Crida & Charnoz 2012) and evolution (Lainey 2008; Lainey et al. 2009) of these bodies. In addition, it brings important links and constraints to the formation and evolution of the Solar system (Nogueira, Brasser & Gomes 2011). Dynamics knowledge also improves ephemerides, allowing for the astrophysical investigation of natural satellites in other rich ways, such as in space exploration and through stellar occultations.

When *Voyager II* visited Uranus' moons in 1986 (Smith et al. 1986), the solar sub-point was in their southern hemispheres. Now their equators and north parts are visible. This raises interest for studies on the newly illuminated surfaces of these bodies. Are they different from the south? Are there new features that can tell us more about the forces and physics that modelled the satellites' surfaces? These topics are in the scope of future space probe missions to be launched from 2030 on, to arrive at the Uranus system from 2040 on (Hofstadter et al. 2019). Ephemeris work is crucial for the planning and successful execution of missions in the spacial exploration of moon systems.

Stellar occultations add great physical knowledge to Solar system bodies in general and to natural satellites alike (Sicardy et al. 2006a,b; Widemann 2009; Morgado et al. 2019a). Accurate and precise shape, size and albedo measurements of the moons, and also the exploration of their surrounding environments, including

\* E-mail: massaf@astro.ufrj.br

atmospheres, can be made from the ground independently of the phase angle illumination of the Sun. The success in observing a stellar occultation at the right time and place depends upon good predictions, which rely on accurate and precise star positions and ephemerides (Assafin et al. 2010, 2012; Benedetti-Rossi et al. 2014; Camargo et al. 2014; Gomes-Júnior et al. 2015, 2016). There is even an important feedback to the body's own ephemeris whenever a stellar occultation is successfully observed, because the method itself is also a source of accurate astrometric information (Desmars et al. 2015).

Improving the orbit and ephemeris demands systematic astrometry of the satellites over extended periods of time, with accurate and precise measurements of positions, relative distances and other observables. These measurements are fitted against the theory with the use of dynamical models (Lainey et al. 2009). Unfortunately, for some years now and for more to come, all the traditional astrometric methods for measuring satellites are facing difficulties in the case of the Uranus system. No probes will fly by or orbit the system until at least 2040 (Hofstadter et al. 2019), preventing space astrometry. Also, the planet has been slowly passing through a sky region without many stars for some time now, and will be for the next five years. For this reason, no feasible stellar occultations are foreseen in the near future for Uranus' satellites. This also impacts the efficiency of the usual methods of CCD astrometry.

Standard CCD astrometry succeeds whenever the satellites are well imaged and there is an adequate number of reference catalogue stars to map distortions in the field of view (FOV). However, this is usually not the case in the observations of Uranus' moons. This is because Miranda ( $R \simeq 16$ ) is usually close to Uranus ( $R \simeq 6$ ), and due to the 2007 equinox, Ariel ( $R \simeq 14$ ), and to a lesser extent also Umbriel ( $R \simeq 15$ ), are passing close to the planet's disc too. We must therefore use long-focus telescopes to obtain a better spacial resolution, but this constrains the FOV to a few arcminutes in size, limiting the number of available stars. We must also take very short exposures to minimize light contamination from the planet, but as a collateral effect we underexpose most of the stars. In practice, only a few usable stars remain, usually not in enough numbers and not uniformly distributed in the FOV. This degrades the FOV distortion mapping and prevents us from obtaining accurate and precise right ascensions and declinations, even with the use of *Gaia*. When enough reference stars are available, as was the case a few years ago, and taking relative positions with respect to Oberon, this classic CCD astrometry method reaches for each coordinate a relative position precision of about 100 mas for Miranda and 50 mas for the other satellites (Camargo et al. 2015). Recently, using a larger FOV and the *Gaia* DR1 catalogue, Xie et al. (2019) reported observations made between 2014 and 2016, with Miranda–Oberon relative position errors of about 45 mas.

Mutual phenomena furnish precise relative positions between two satellites. They occur during the equinox of the host planet, when the Earth and the Sun cross the orbital plane of the satellites. In such a geometric configuration, occultations and eclipses between pairs of satellites can be observed from the Earth. As one satellite (or its projected shadow in the case of an eclipse) hides another satellite, the drop in the light flux can be measured with high precision by differential photometry. The light curve obtained keeps information about the apparent relative motion between the satellites in the plane of sky. From the analysis of the observed light curve, the central instant at closest approach is determined, as is the minimum apparent distance – the impact parameter – and the relative velocity. The central instant and impact parameter can be expressed in terms of right ascension and declination differences between the satellites.

The last Uranus equinox in 2007 was in fact the first time that mutual phenomena were actually observed for this system. High-precision relative satellite positions were published with errors of about 20 mas on each coordinate for just a few tens of events (Hidas, Christou & Brown 2008; Assafin et al. 2009; Arlot et al. 2013). Since the orbital period of Uranus is about 84 yr, there is an equinox only every nearly 42 yr, so unfortunately the next equinox will only occur in 2050.

Therefore, it is important to develop alternative methods that can still furnish high-quality astrometric data for Uranus' satellites. For example, Peng et al. (2012a) determined relative positions between pairs of satellites close together in the FOV and achieved a precision of 30 mas for the Jovian moons. The so-called *precision premium* (Peng et al. 2008) predicts an increase in the precision in the measurement of apparent distances between two objects in the sky plane when this distance is smaller than 85 arcsec. In this scenario, we avoid the effects of astronomical and instrumental distortions in the FOV, since both satellites are affected in the same way. This is most true for the Uranus system, since relative distances are never greater than 60 arcsec.

In this context, a very promising technique is mutual approximations. Developed by Morgado et al. (2016), the technique was primarily suggested by Arlot et al. (1982). This new method can accurately and precisely furnish the central instant at closest apparent approach between two moving satellites in the sky plane. Measurements are made on very small portions of the FOV and benefit from the *precision premium*. The central instant is independent of reference star positions and can be directly used in orbital or ephemeris computational work (Emelyanov 2017; Morgado et al. 2019b). This technique is actually inspired by mutual phenomena and shares the same geometric principles and parameters. First applications to the Jovian moons (Morgado et al. 2016, 2019b) indicate that it achieves comparable precision in the central instant. However, unlike mutual phenomena, mutual approximations occur at virtually any time outside equinoxes. The central instant is obtained without the need to calibrate or scale the measured instrumental ( $x, y$ ) coordinates in pixels. The method profits from the accurate recording of time, which can be easily done by using GPS receivers or calibrated internet time.

In this paper we present results for 23 mutual approximations involving the five main Uranus satellites: Miranda, Umbriel, Ariel, Titania and Oberon. A total of 15 873 observations were made with the 1.6 m aperture telescope of Pico dos Dias Observatory (OPD) in Brazil during 2015–2018. Images were digitally coronagraphed to attenuate the scattered light from Uranus, improving measurements for Miranda, Ariel and Umbriel. Unlike in Morgado et al. (2016, 2019b), we were able to derive the pixel scale and CCD orientation angle by using the ephemerides and measured distances of the other nearby satellites in the FOV not involved in the approximation. In this way, by developing a variant of the usual mutual approximations method, we managed to measure the impact parameter in mas (not in pixels) and relative velocities in  $\text{mas s}^{-1}$  for the first time, also obtaining distance and relative velocity inter-satellite components in right ascension and declination in the International Celestial Reference System (ICRS).

Section 2 describes the variant of the method of mutual approximations developed. A guide to using the outputs of the method as observables in orbit and ephemeris computational work is also given. In Section 3 we describe the criteria for the selection of the events, the instruments used and observations. In Section 4 we detail the image treatment, consisting of the digital coronagraphy and ( $x, y$ ) centroid measurements. In Section 5 we give information about

the data fitting of ephemerides and observed distance and relative velocity curves. In Section 6, we show and analyse our results. We give comments and conclusions in Section 7.

## 2 MUTUAL APPROXIMATIONS

On the lack of reference objects in the FOV, there are only two ways in mutual approximations to determine the impact parameter and relative velocity in units of mas and  $\text{mas s}^{-1}$  respectively, instead of expressing them in useless pixel units. One is by setting the pixel scale from the observation of nearby sky fields with catalogue stars in the ICRS, although this does not usually render accurate astrometric results. The other way is to use the ephemerides of the actual pair of target satellites (Peng et al. 2012a), which demands care to avoid possible correlations with the ephemerides' errors of the actual targets. In this case, the ephemerides represent the ICRS. This situation is common in the observation of the bright, more widely spread Jovian moons, when frequently only two Galilean satellites are present in a FOV of typically a few arcminutes in size. No reference stars are found or are badly underexposed due to the necessarily short exposures. In this case, only the central instant can be obtained in the usual ways by the method of mutual approximations as described in Morgado et al. (2016, 2019b), where the ICRS is represented by the UTC timing of the observations.

The observational circumstances of Uranus' moons are similar. We must also do short exposures to avoid the contamination of Miranda, Ariel and Umbriel by the planet's light. We are forced to use long-focus telescopes with a smaller FOV, the distortion of which may not be proportionally smaller and thus not adequately mapped with the loss of reference stars. To make things worse, the current sky path of Uranus itself presents a very low star density. Therefore, in practice, we also frequently run out of reference stars, as in the case of the observation of the Jovian moons.

However, there is one crucial difference. Unlike the Jupiter system, we usually have all five main Uranus moons available in the FOV, which can be as small as about 1 arcmin in size, because the inter-satellite distances never exceed 60 arcsec. This allows for computation of the pixel scale in  $\text{mas pixel}^{-1}$  using the same image of the targets, but not using in common their  $(x, y)$  measurements and ephemerides. Instead, we use the  $(x, y)$  measurements and ephemerides of any two of the other moons present in the FOV. Besides the pixel scale, the CCD orientation angle that gives the  $(\alpha, \delta)$  axes can also be computed. Moreover, the pixel scale and orientation angle are determined under the beneficial astrometric properties of the *precision premium*. In this way, besides the central instant, we are able to obtain the impact parameter in mas and relative velocity in  $\text{mas s}^{-1}$  without reference stars and not based on the ephemerides and measurements of the target satellites. We notice, however, that some correlation between the targets and separate satellites will always exist. Their ephemerides share some common parameters, like the mass of the primary (Vienne, Thuillot & Arlot 2001). They are also affected by some common systematic errors of observational origin, propagated by classical  $(\alpha, \delta)$  astrometry work. Although the distance is always a concern in the precise computation of the pixel scale and CCD orientation angle (Peng et al. 2008, 2012a), we will see that the typical apparent distances in the FOV between the satellites in the Uranus system are enough to render excellent results (see Section 5). The ICRS system is again represented by the UTC timing and also by the ephemerides used.

In this new context, unlike in Morgado et al. (2016, 2019b), we present in Section 2.1 a variant of the method of mutual

approximations, developed and used in this work, which is suited for the case when, besides the mutual approximation satellites, a separate pair of satellites is also available in the FOV. We determine the central instant, the impact parameter in mas and the relative velocity in  $\text{mas s}^{-1}$  at the central instant. From them, we also compute the inter-satellite distances  $(X, Y)$  and relative velocities  $(\dot{X}, \dot{Y})$  in  $(\alpha, \delta)$  components at the central instant. Observed distances in mas for each individual observation are also obtained, but not in the context of Peng et al. (2012a), since here the results are truly independent of the  $(x, y)$  measurements of the targets and are not based on their ephemerides. From the computed pixel scale and CCD orientation angle, inter-satellite distances  $(X, Y)$  in mas are also derived for each individual observation. In Section 2.2 we show how the pixel scale and orientation angle are obtained. In Section 2.4 we guide the reader on how to use the results derived from this variant of the method of mutual approximations – the central instant, impact parameter, relative velocity, inter-satellite distances and velocities at the central instant, individual inter-satellite distances – as observables in orbit and ephemeris fitting work. All the procedures in Sections 2.1, 2.2 and 2.3 for the reduction of observations made with this variant of the method of mutual approximations were implemented as a new task in the PRAIA package (Assafin et al. 2011), with the help of SOFA libraries (SOFA 2018). Ephemerides were generated by another PRAIA task with the use of NASA's Navigation and Ancillary Information Facility (NAIF) SPICE toolkit (Acton 1996).

### 2.1 Central instant, impact parameter, relative velocity, $(\alpha, \delta)$ inter-satellite distances and velocities

The method of mutual approximations relies on the same geometry that describes mutual phenomena in the plane of the sky (Assafin et al. 2009; Dias-Oliveira et al. 2013). The instant at maximum approximation when the apparent distance is at a minimum is the central instant  $t_0$ . The minimum apparent distance in the sky plane between both satellites, which occurs by definition at  $t_0$ , is the impact parameter  $d_0$ . The apparent relative velocity  $v_0$  in the sky plane at  $t_0$  is the total relative velocity between both satellites.

For the short orbital arcs of the events, the apparent relative motion of the satellites, i.e. the distance and relative velocity curves, can be accurately described by polynomials in time of degree  $N$ . For computational convenience, we internally use the squares of distances and relative velocities in all fittings, but recover the usual non-squared values in the results, errors, plots and analysis in general (Morgado et al. 2016, 2019b). We can construct ephemeris curves from the  $(\alpha, \delta)$  ephemeris of the satellites, or observed curves from their  $(x, y)$  observations. Using the least-squares method, we fit distance curves by a polynomial, find the minimum and get  $t_0$  and  $d_0$ . From the polynomial fittings to velocity curves, we get  $v_0$  at  $t_0$ . Measurement errors for each observed distance and relative velocity are estimated from the  $(x, y)$  measurement errors, and can be used as weights in the least-squares computations of observed curves. Ephemeris curves are fitted without weighting. From the polynomial fittings of observed curves, errors are assigned to  $t_0$ ,  $d_0$  and  $v_0$  from the values and errors of the fitted coefficients.

The degree of the polynomial is set by testing different even values from 2 to 8 in the fit of the ephemeris distance curve, until the mean error of the fit equals a truncation threshold of 1 mas. It is usually 2 and rarely 4. We can set the minimum time baseline for the computation of individual velocities, so as to avoid problems with too-slow relative velocities. In slow relative velocity regimes, larger baselines give sounder velocity values, but at the cost of

smaller numbers of individual velocities available in the relative velocity curve. The maximum number of individual points in a relative velocity curve is by construction half the number of points in a distance curve, or half the number of observed images. This number diminishes as we increase the time baseline of the velocity curve. For the slow 0.1–0.8 mas s<sup>-1</sup> relative velocities of Uranus' moons, typically a 30–60 min time baseline will do.

The central instant is obtained in UTC. For the evaluation of  $t_0$  errors and  $\Delta t_0$  ephemeris offsets, conversion from seconds to milliarcseconds is made by using the ephemeris relative velocity  $v_0$  at  $t_0$ . The  $d_0$  and  $v_0$  values and errors are converted from pixels and pixels s<sup>-1</sup> to mas and mas s<sup>-1</sup> by the use of the pixel scale computed as in Section 2.2.

The ephemeris distance and relative velocity curves are not constrained by the observed instants. They cover the event uniformly and symmetrically around the central instant. The fitted  $t_0$ ,  $d_0$  and  $v_0$  ephemeris values are thus unaffected by possible gaps and uneven distribution of the points in the real observed curves. They are used in the comparisons with observations to derive ephemeris offsets  $\Delta t_0$ ,  $\Delta d_0$  and  $\Delta v_0$ . We use two types of topocentric ephemeris: astrometric and apparent. The apparent ephemeris is affected by solar phase angle effects, light deflection, light time, aberration and atmospheric refraction. We must use a reflectance law for the computation of solar phase angle effects. The PRAIA task offers two options: Lambert (Lindgren 1977) and Lommel–Seeliger (Hestroffer 1998) reflectance laws. In Section 5 we indicate which one was used in this work. From the two sets of  $t_0$ ,  $d_0$  and  $v_0$  values obtained from fitting ephemeris curves with these two ephemeris types, we derive conversion factors to transform apparent observed topocentric  $t_0$ ,  $d_0$  and  $v_0$  values to their corresponding astrometric observed topocentric ones, as explained in Section 2.3.

The inter-satellite observed astrometric topocentric distances ( $X \equiv \Delta\alpha \cos \delta$ ,  $Y \equiv \Delta\delta$ ) and relative velocities ( $\dot{X}$ ,  $\dot{Y}$ ) in  $(\alpha, \delta)$  components at  $t_0$  are computed with the knowledge of the position angle  $\theta$  in the sky plane of satellite 1 with respect to satellite 2 at the central instant. This angle  $\theta$  (anticlockwise, zero toward east) is easily computed from the astrometric topocentric ephemerides of the satellites. Observed  $(X, Y)$  are determined straightforwardly by adding the known ephemeris astrometric topocentric  $(X_{\text{ep}}, Y_{\text{ep}})$  at  $t_0$  to the astrometric topocentric ephemeris offsets  $(\Delta X, \Delta Y)$  in the sense ‘observed minus ephemeris’. Ephemeris offsets  $(\Delta X, \Delta Y)$  are in turn obtained from the corresponding ephemeris offsets in central instant  $\Delta t_0$  and impact parameter  $\Delta d_0$  as in equations (1). By convention, the relative velocity  $v_0$  is set negative/positive when it points toward increasing/decreasing  $\theta$  at  $t_0$  in equations (1). The  $(X, Y)$  errors are evaluated from the  $t_0$  and  $d_0$  errors applied to equations (1). Observed astrometric topocentric relative velocities  $(\dot{X}, \dot{Y})$  are obtained by multiplying  $v_0$  respectively by  $\sin \theta$  and  $\cos \theta$ , and taking the correct signs, after evaluating the ephemeris astrometric topocentric relative velocity  $(\dot{X}, \dot{Y})$  component signs. The  $(\dot{X}, \dot{Y})$  errors are the same for each coordinate and their root mean square equals the total error in  $v_0$ :

$$\begin{aligned} \Delta X &= \Delta d_0 \cos \theta - \Delta t_0 v_0 \sin \theta \\ \Delta Y &= \Delta d_0 \sin \theta + \Delta t_0 v_0 \cos \theta. \end{aligned} \quad (1)$$

Individual observed apparent  $(X_{12}, Y_{12})$  inter-satellite distances for the approximation satellites in the sense ‘satellite 1 minus 2’ are computed in mas from their measured distances in pixels  $(x_{12}, y_{12})$ , in accordance with equations (2). For that, we use the pixel scale  $p$  and CCD orientation angle  $\Omega$  first determined as explained in Section 2.2, where  $k$  is set to +1 for right-handed or -1 for left-

handed CCD  $(x, y)$  coordinate systems. Then, the apparent  $(X_{12}, Y_{12})$  distances are finally converted to individual observed astrometric topocentric  $(X, Y)$  inter-satellite distances, by applying conversion factors derived from the astrometric and apparent ephemerides of the satellites (see Section 2.3):

$$\begin{aligned} X_{12} &= +kpx_{12} \cos \Omega + kpy_{12} \sin \Omega \\ Y_{12} &= -kpx_{12} \sin \Omega + kpy_{12} \cos \Omega. \end{aligned} \quad (2)$$

## 2.2 Pixel scale and CCD orientation angle

The pixel scale and CCD orientation angle are computed by using any two nearby separate satellites present in the FOV, other than the two satellites in the approximation. They are thus not based on the ephemerides and  $(x, y)$  measurements of the target satellites, but are computed with the same images and under the benefits of the *precisium premium*.

For each observation instant, we extract the apparent ephemeris of both separate satellites, affected by solar phase angle effects, light deflection, light time, aberration and atmospheric refraction.

The pixel scale is determined in mas pixel<sup>-1</sup> by taking the average of the ratios between apparent ephemeris and measured distances of the satellites chosen for this task, weighted by the observed distance errors, with outliers eliminated in a sigma-clip procedure, using a given sigma factor (usually 2.5 or 3.0; see the value used in this work in Section 5). The pixel scale error is the standard deviation about that average.

The CCD orientation angle  $\Omega$  of the  $(\alpha, \delta)$  axes with respect to the  $(x, y)$  ones is determined from the apparent ephemeris  $(X_{\text{ep}}, Y_{\text{ep}})$  and observed  $(x_{\text{ob}}, y_{\text{ob}})$  inter-satellite distances in accordance with equations (3), where  $k$  is set as in equations 2 in Section 2.1. The angles are computed for each image and weighted by the observed distance errors. We take the same images used in the determination of the pixel scale. The CCD orientation angle is the weighted mean of all computed values in degrees. Its error is the standard deviation about that mean, usually given in arcseconds:

$$\begin{aligned} \cos \Omega &= \frac{y_{\text{ob}} Y_{\text{ep}} + k x_{\text{ob}} X_{\text{ep}}}{x_{\text{ob}}^2 + y_{\text{ob}}^2} \\ \sin \Omega &= \frac{y_{\text{ob}} X_{\text{ep}} - k x_{\text{ob}} Y_{\text{ep}}}{x_{\text{ob}}^2 + y_{\text{ob}}^2}. \end{aligned} \quad (3)$$

The pixel scale and CCD orientation angle are obtained with apparent topocentric coordinates affected by solar phase angle effects, light deflection, light time, aberration and atmospheric refraction. They are not defined in the astrometric topocentric frame. For deriving astrometric topocentric distances and velocities, conversions must be made as explained in Sections 2.1 and 2.3.

## 2.3 Conversion from apparent to astrometric observed central instants, distances and relative velocities

Since we do not have individual satellite positions from observations, but only distances and relative velocities between satellite pairs, we cannot convert observed apparent values to astrometric ones using standard formulae and procedures. On the other hand, we can do that with ephemeris positions, and from that derive astrometric and apparent central instants, distances and relative velocities between any two satellites. Thus, from both astrometric and apparent ephemeris sets of central instants, distances and relative velocities, we can compute factors that can be applied to convert observed apparent values in astrometric ones.

For the conversion of central instants, we simply take the difference between the astrometric and apparent values obtained from the distance curve fittings of the corresponding ephemerides. We add this difference to the observed central instant in order to obtain the observed astrometric central instant.

For the impact parameter, the conversion factor is the ratio between the astrometric and apparent impact parameters computed from the distance curve fittings of the respective ephemerides. We multiply this factor by the observed impact parameter to obtain the astrometric impact parameter.

For the relative velocity, the conversion factor is the ratio between the astrometric and apparent relative velocities computed from the relative velocity curve fittings of the corresponding ephemerides. We multiply this factor to the observed relative velocity to obtain the astrometric relative velocity.

For the inter-satellite  $(X, Y)$  coordinates and relative velocities  $(\dot{X}, \dot{Y})$  at the central instant  $t_0$ , and for the  $(X, Y)$  coordinates of each individual observation, the respective conversion factors are obtained by the same kind of ratio computation done for the impact parameter and relative velocity, but separately for the respective  $X$  and  $Y$  components. In the case of individual  $(X, Y)$  coordinates, we fit separate ephemeris curves in  $X$  and  $Y$  to derive conversion factors in  $X$  and  $Y$  at each observed instant. Finally, we multiply the conversion factors found for each  $X$  and  $Y$  component by the corresponding observed values to obtain the astrometric ones.

#### 2.4 Using central instants, impact parameter, relative velocity, $(\alpha, \delta)$ inter-satellite distances and velocities in orbit/ephemeris fitting

In the case of natural satellites, orbit and ephemeris fitting of dynamical models to observations is done by using the standard method of variational equations (see e.g. Lainey, Arlot & Vienne 2004a; Lainey, Duriez & Vienne 2004b). How do we turn all the outputs of the variant of the method of mutual approximations used in this work – central instants, impact parameter, relative velocity,  $(\alpha, \delta)$  inter-satellite distances and velocities – into useful observables by developing adequate conditional equations? What is the best approach to use them?

If only the central instant is available, or is to be fitted, the appropriate procedure is already described in detail by Morgado et al. (2019b) (Section 5), including explicit conditional equations. For all the other mutual approximation outputs, which can be reduced to distances or relative velocities in one or two dimensions, standard conditional equations are readily available in the literature (see Emelyanov 2017, and references therein).

Emelyanov (2017) gives a thorough revision on the subject, including the development of useful condition equations for one- and two-dimensional observables, with references about this subject. Through simulations, he also points out the best strategies for using distinct and mixed sets of observables.

Emelyanov evaluated the mutual approximations as they were applied by Morgado et al. (2016), with only the contribution of central instants, which is a particular kind of one-dimensional observable. He concluded that the method is promising once we mix the central instant with other one- and two-dimensional observables in the orbit fittings.

Emelyanov also concluded that the best individual contributions come from two-dimensional orthogonal sets, like  $(\alpha, \delta)$  relative positions and central instants with impact parameters from mutual phenomena. Notice that these are exactly the observables that we derive with the variant of the mutual approximations method

developed in Section 2.1: central instants with the impact parameter, inter-satellite  $(X, Y)$  coordinates and even  $(\dot{X}, \dot{Y})$  relative velocities at  $t_0$ , not to mention individual distances and inter-satellite  $(X, Y)$  coordinates.

Finally, the use of all these kinds of sets of observables together is strongly recommended by Emelyanov (2017) as the best strategy of all. Thus, thanks to the determination of the pixel scale and orientation angle, and to the *precision premium*, we must conclude that the observables generated by the variant of the mutual approximations method are in full compliance with the best practices in orbital and ephemeris work.

### 3 SELECTION OF EVENTS AND OBSERVATIONS

We selected only mutual approximations when, by the time around the predicted event, the satellites presented angular distances greater than 7 arcmin to the limb of Uranus, 30° to the Moon's, and zenith distances smaller than 55°. We used the JPL DE432 + URA111 ephemerides in the computations. The predictions of the approximations were made with apparent topocentric ephemerides generated with NASA's NAIF/SPICE toolkit (Acton 1996), using the same PYTHON-based software (Astropy Collaboration et al. 2013) developed for the Jupiter's Galilean Moons in Morgado et al. (2016), adapted for the five Uranus main satellites.

Observations were made with the 1.60 m aperture  $f/10$  Perkin-Elmer telescope (Ritchey-Chrétien optics), located at the Pico dos Dias Observatory (OPD) run by Laboratório Nacional de Astrofísica/MCTI,<sup>1</sup> Itajubá/MG, Brazil, IAU code 874. The geographical longitude, latitude and altitude are 45°34'57.5' W, 22°32'07.8' S and 1864 m. A 2Kx2K pixel Andor/iKon CCD detector was used resulting in a FOV of 6 arcmin in size. The last two events were observed with a different CCD, an Andor/iXon model with half the FOV. Images were stored in FITS format. The UTC time was input in the FITS headers by a GPS receiver with errors below 0.1 s. In all observations, Uranus and the satellites were kept in the central part of the CCD frame to attenuate the effects of FOV distortions, if any (see Peng et al. 2012b). An  $I$  filter compatible with the Johnsons-Cousins system was used in all observations to mitigate colour refraction effects, resulting in an effective wavelength of 0.800  $\mu\text{m}$ . We took 5-s exposures at least one hour before and after the predicted central instant. However, due to weather or instrumental issues, some of the observation series were incomplete, resulting in absent parts in some of the distance and velocity curves, usually gaps. A few times, a portion of the curve is lacking before or after the central instant (distance and relative curve plots for all events are available as online supporting information).

Including a pilot test in 2015, we were able to successfully register 23 mutual approximations, some of them observed on the same night. A dozen other events were lost due to bad weather or critical instrumental issues in the observations that could not be overcome. A total of 15 873 useful individual CCD images were acquired, about 690 per event. For each approximation, we present in Table 1 all the relevant observation information for the computations described in Section 2.1: solar phase angle, zenith distance, pressure, temperature and humidity. The position angle  $\theta$  as defined in Section 2.1 was computed from the ephemerides of the target satellites. The pixel scale  $p$  and CCD orientation angle  $\Omega$  (and errors) were computed for each event following the prescriptions in

<sup>1</sup><http://www.lna.br/>, in Portuguese

**Table 1.** Observational information for the 23 mutual approximations between Uranus' moons.

Date	Sats	$i$ ( $^{\circ}$ )	$z$ ( $^{\circ}$ )	$P$ (mBar)	$T$ ( $^{\circ}\text{C}$ )	$U$ (per cent)	$\theta$ ( $^{\circ}$ )	$p$ (mas/pixel)	$\sigma p$ (mas/pixel)	$\Omega$ ( $^{\circ}$ )	$\sigma\Omega$ (arcsec)	paSats	Images
2015 Oct. 13	MU	0.06	38.46	1009.09	20.2	56	345.027	176.672	0.001	182.78	70	TO	433
2016 Aug. 23	UT	2.34	32.41	1018.53	6.0	91	191.294	177.033	0.004	177.07	225	AO	1015
2016 Sept. 10	MA	1.69	36.54	1015.33	11.4	95	017.780	176.606	0.001	179.52	65	TO	1024
2016 Sept. 10	MT	1.69	31.97	1015.33	11.4	95	222.997	176.552	0.001	179.53	104	AO	971
2016 Sept. 11	MO	1.65	34.96	1014.80	12.3	92	142.128	176.617	0.002	179.51	99	AT	652
2016 Sept. 23	AU	1.12	33.98	1013.60	11.1	70	200.441	176.419	0.002	179.03	95	TO	837
2016 Nov. 3	MT	0.95	40.93	1011.47	13.2	96	284.945	176.597	0.002	178.97	269	AO	675
2017 Aug. 10	MU	2.75	49.54	1010.00	15.1	66	340.875	176.431	0.001	180.17	89	TO	472
2017 Aug. 10	MT	2.75	46.59	1010.00	15.1	66	344.224	176.547	0.001	180.18	112	AO	512
2017 Aug. 10	UT	2.75	38.10	1010.00	15.1	66	346.382	176.547	0.001	180.18	112	AO	1065
2017 Aug. 10	MA	2.75	36.55	1010.00	15.1	66	188.139	176.431	0.001	180.17	89	TO	1040
2017 Aug. 11	MA	2.73	33.89	1014.13	15.5	22	024.423	176.314	0.002	180.16	120	TO	601
2017 Aug. 15	AO	2.66	45.27	1010.67	14.2	90	188.778	176.626	0.003	180.13	147	UT	570
2017 Aug. 15	MO	2.66	33.01	1010.67	14.2	90	191.887	176.626	0.003	180.13	147	UT	564
2017 Aug. 15	AT	2.66	32.92	1010.67	14.2	90	200.166	176.579	0.002	180.15	133	UO	694
2017 Oct. 18	AT	0.09	37.42	1015.73	14.0	86	307.557	176.621	0.002	181.16	90	UO	376
2017 Nov. 13	UT	1.22	49.57	1006.13	12.3	67	306.871	176.738	0.005	185.07	144	AO	655
2018 July 16	AT	2.90	48.45	1015.46	11.8	73	001.343	176.494	0.002	178.59	81	UO	400
2018 July 17	MU	2.90	39.39	1017.86	11.1	67	095.414	176.511	0.003	178.57	121	TO	388
2018 July 18	AT	2.91	49.36	1015.60	9.8	90	094.352	176.342	0.003	178.63	238	UO	790
2018 Aug. 19	TO	2.67	37.45	1016.13	8.6	97	333.142	176.714	0.006	180.49	147	AU	994
2018 Sept. 28	MA	1.29	40.06	1007.07	17.3	70	277.284	168.632	0.002	88.12	90	TO	324
2018 Oct. 22	AT	0.10	40.10	1010.93	9.6	97	095.073	170.286	0.001	90.26	183	TO	821

*Note:* The four blocks of the table refer to 2015, 2016, 2017 and 2018 events respectively. ‘Sats’ stands for the satellites in mutual approximation, A = Ariel, U = Umbriel, T = Titania, O = Oberon, M = Miranda.  $i$ ,  $z$ ,  $P$ ,  $T$  and  $U$  refer to the solar phase angle, zenith distance, pressure, temperature and humidity respectively. The position angle  $\theta$  as defined in Section 2.1 was computed from the ephemerides of the target satellites. ‘paSats’ refers to the satellites used in the computation of the pixel scale  $p$  with error  $\sigma p$ , and CCD orientation angle  $\Omega$  with error  $\sigma\Omega$ . ‘Images’ refers to the number of observations effectively used after elimination of outliers in the distance fittings (see Section 6). The last two events were observed with a different CCD detector, mounted on different camera supports on each night, which resulted in the distinct pixel scales and orientation angles listed.

Section 2.2 (see also Section 5) and are listed in advance in Table 1. The number of images listed per event refers to the observations effectively used after elimination of outliers in the distance fittings (see Section 5). The orbital coverage of the approximation satellites around Uranus for the nights of the 23 observed approximations is illustrated in Fig. 1. The satellites are evenly distributed along their orbits, except Oberon with few approximations. Miranda was involved in 12 approximations, Ariel 11, Umbriel 7, Titania 12 and Oberon 4. The radii for the satellites used in this work were taken from Thomas (1988). For Ariel and Miranda, which present a triaxial form, a mean value was assumed, as in Assafin et al. (2009). The values were 236.0, 579.0, 584.7, 788.9 and 761.4 km for Miranda, Ariel, Umbriel, Titania and Oberon respectively.

#### 4 DIGITAL CORONAGRAPHY AND CENTROID MEASUREMENTS

All acquired images were first corrected for bias and flat-field (no dark correction was necessary) using standard IRAF<sup>2</sup> procedures (Butcher & Stevens 1981). The image treatment started with digital coronagraphy and finished with the measurement of the  $(x, y)$  centroids. It was entirely done with the tasks of the PRAIA astrometric and photometric package (Assafin et al. 2008, 2011).

In Assafin et al. (2009) and Camargo et al. (2015), a detailed description of the digital coronagraphy image processing, including graphic examples, and its impact on the photometry and astrometry of Uranus’ moons can be found. The digital coronagraphy serves to minimize the influence of the planet’s light in the astrometric

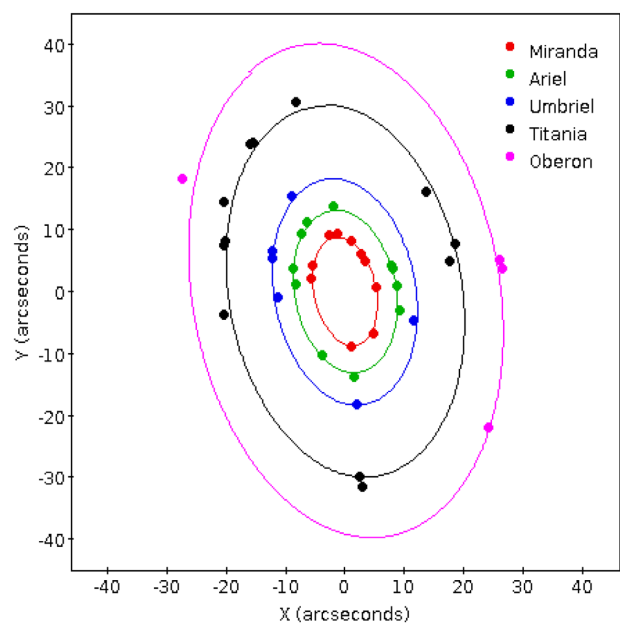


**Figure 1.** Satellite places (dots) in their orbits around Uranus projected in the sky plane on the nights of observation of their mutual approximations. The reference orbits were drawn at the middle epoch 2017.5.

measurements of the satellites, mostly Miranda but also Ariel and Umbriel, usually embedded in the scattered light of Uranus. The critical part consists of computing the light profile of the bright object. It is computed pixel by pixel, by sampling planet-centred

<sup>2</sup><http://iraf.noao.edu/>

rings passing at each pixel in an iterative procedure around the planet, then over the entire image. After the planet's light profile is computed, it is subtracted from the original data, resulting in a new image, digitally coronagraphed. This procedure recovers the symmetry of the light profiles of the satellites, bent over Uranus in the original images. It also permits the computation of their correct flux and signal-to-noise ratio (SNR).

The moving satellites are automatically tracked and measured in the images. The  $(x, y)$  centroids are measured by the fit of pixels to a two-dimensional circular Gaussian profile.

Usually in most astrometric packages and routines, the pixels subject to fitting are within a circular region of radius  $2.5 \times$  the Gaussian  $\sigma$ , or about 1 FWHM (1 full width half maximum = seeing). In the usual iterative procedure, as the centre is refined and a new  $\sigma$  is computed for the Gaussian, the region is also recentred and resized until convergence is reached.

In this work, we fitted pixels in a new improved and more robust manner, as is now available in the PRAIA package. In an iterative procedure involving aperture photometry, the circular region centre and size are sampled, as well as the radius and width of a surrounding sky background ring. The selected region is that for which the photometric SNR is highest. Two-dimensional circular Gaussian fittings are performed many times during the process, until the circular region is finally set and the final  $(x, y)$  is found. Tests indicate an improvement of about 10–30 per cent in the precision of the  $(x, y)$  measurements, with excellent performance even under bad seeing and for underexposed objects. Other improvements in the  $(x, y)$  measurements of the PRAIA package were implemented in its recent upgraded version, but their description is beyond the scope of this text.

## 5 DISTANCES, RELATIVE VELOCITIES, CURVE FITTING

Following the procedures described in Sections 2.1 and 4,  $(x, y)$  measurements and errors, observed distances, relative velocities and respective internal errors were computed for all images of all 23 mutual approximations observed. The relative velocities were calculated by picking up distance measurements separated in time by about 30–60 min depending on the specific relative velocities, which were always slower than  $0.8 \text{ mas s}^{-1}$ . The JPL ephemerides DE432 + URA111 were used in all computations: construction of ephemeris curves for distance and relative velocity, pixel scale, orientation angle,  $(\alpha, \delta)$  inter-satellite distances and relative velocities, and conversion factors between apparent and astrometric topocentric coordinates. For that, we used the auxiliary data displayed in Table 1. In the solar phase angle computations, we tested both Lambert and Lommel–Seeliger reflectance laws. They gave the same values within about 1 mas. For its simplicity, all the results shown here refer to the Lambert law. Typical  $(x, y)$  measurement errors for Miranda were 30 mas and 10 mas for the other satellites. Seeing typically varied between 1.5 and 2 arcsec.

In the pixel scale and CCD orientation angle computations (Section 2.2), we used the two other satellites present in the FOV, as indicated in Table 1, but never Miranda, always taking satellites with the best  $(x, y)$  measurements available. In these computations, we used a  $3.0\sigma$  factor in the sigma-clip procedures for the elimination of outliers. An approximation satellite, Titania, was exceptionally used for the 2018 October 22 event because only one separate satellite was available and it formed with Titania the most distant satellite pair. Computed values and errors for pixel scale  $p$  and orientation angle  $\Omega$  are listed in Table 1. In some cases we used other satellites

in the computations to compare the precision, and found that the pixel scale and orientation angle obtained were fairly similar, well within  $1\sigma$  errors, even when not using the most distant satellite pairs.

A second-degree polynomial was used to fit the ephemeris and observed distance and velocity curves (see Section 2.1). For the events of 2016 September 106, 2017 August 10 (that with Miranda and Ariel), and 2017 August 11 the fourth degree was used. The mean errors of the distance and relative velocity polynomial fittings were 40 mas and  $0.01 \text{ mas s}^{-1}$  respectively. Using a sigma-clip procedure, we discarded about 6 and 9 per cent of outlier points above  $3.0\sigma$  in the distance and relative velocity curve fittings respectively. The total number of used individual distances for all 23 events was 15 873 with an average of 690 fitted points per event, and 8871 points with 385 per event on average for the relative velocity fittings.

## 6 RESULTS AND ANALYSIS

We present results for 23 mutual approximations between the main moons of Uranus successfully observed between 2015 and 2018. The results relating to the fitting of distance curves are given in Table 2 and those to relative velocity in Table 3. The tables contain the event date and the pair of satellites involved. Table 2 presents the astrometric topocentric central instant  $t_0$  in UTC and the impact parameter  $d_0$  in mas. Converted from the central instant and impact parameter,  $X$  and  $Y$  astrometric topocentric inter-satellite  $(\alpha, \delta)$  distances in the sense ‘satellite 1 minus 2’ in mas ( $\cos \delta$  applied for  $X$ ) are also listed in Table 2 at  $t_0$ . Results for astrometric topocentric relative velocities in  $\text{mas s}^{-1}$  are displayed in Table 3, including  $\dot{X}$  and  $\dot{Y}$  astrometric topocentric inter-satellite  $(1, \delta)$  relative velocities in the sense ‘satellite 1 minus 2’ in  $\text{mas s}^{-1}$  ( $\cos \delta$  applied for  $\dot{X}$ ) at  $t_0$ . In both tables, errors and ephemeris offsets for all these quantities in the sense ‘observed minus ephemeris’ are furnished with their mean and standard deviation (s.d.). We used the JPL DE432 + URA111 ephemerides in all comparisons.

An example of a fitting to an observed apparent distance curve is displayed in Fig. 2, with apparent distances affected by solar phase angle effects, light deflection, light time, aberration and atmospheric refraction. Plots for the distance curves of each of the 23 mutual approximations are available as online supporting information.

According to Table 2, the central instant internal errors were typically below 1 mas, with only one event (2018 July 16) above 10 mas, because of its relatively short and asymmetric distance curve, which starts 5 min before and ends 55 min after  $t_0$ . Only four events had impact parameter internal errors above 25 mas. Considering the 50 mas ( $1\sigma$ ) error, typical of classical CCD relative position astrometry for Uranus’ moons (Camargo et al. 2015), all ephemeris offsets in the central instant are below  $3\sigma$  (150 mas). Events with high internal errors and relatively large ephemeris offsets were affected to some extent by non-ideal weather conditions, such as tenuous passing clouds and relatively high seeing (above 2 arcsec), resulting in distance curves with gaps, some asymmetry and relatively high dispersion due to the low SNR.

For the mutual approximations indicated in Table 2, we plot in Fig. 3 the mutually orthogonal astrometric topocentric ephemeris offsets for central instant and impact parameter. The corresponding plots for  $(\Delta X, \Delta Y)$  ephemeris offsets in  $(X, Y)$  inter-satellite distances ( $\cos \delta$  applied for  $X$ ) are given in Fig. 4. We obtained average central instant and impact parameter internal errors of 0.6 and 14.8 mas respectively, not considering spurious individual errors in the statistics, indicated by ‘\*’ in Table 2. These values

**Table 2.** 23 mutual approximations: results for central instant, impact parameter and  $(X, Y)$  inter-satellite distances at the central instant.

Date	Sat 12	$t_0$ UTC (hhmmss.s)	$\sigma_{t_0}$ (s)	$\Delta t_0$ (s)	$\sigma_{t_0,  v_0 }$ (mas)	$\Delta t_0, v_0$ (mas)	$d_0$ (mas)	$\sigma_{d_0}$ (mas)	$\Delta d_0$ (mas)	$X$ (mas)	$Y$ (mas)	$\sigma_X$ (mas)	$\sigma_Y$ (mas)	$\Delta X$ (mas)	$\Delta Y$ (mas)
Oct. 13	MU	01 06 33.7	2.7	158.9	0.2	+14.1	5743.2	10.5	-6.8	+5548.8	-1482.1	10.1	2.7	-2.9	+15.4
Aug. 23	UT	05 49 34.4	0.6	-141.2	0.4	+83.4	29462.2	7.2	-63.9	-28 897.5	-5740.4	7.1	1.5	+79.0	-69.2
Sept. 10	MA	03 55 17.9	3.5	-3.3	2.9	+2.8	12 206.5	60.8	-36.3	+11 624.9	+3723.1	57.9	18.8	-35.4	-8.5
Sept. 10	MT	04 46 10.8	0.5	+107.9	0.1	+19.9	14922.1	4.9	+6.5	-10910.6	-10 179.9	3.6	3.3	+8.8	-19.0
Sept. 11	MO	06 15 27.2	0.6	+132.2	0.1	+19.9	24750.3	5.1	+21.5	-19 534.9	+15 198.0	4.0	3.1	-29.2	-2.5
Sept. 23	AU	03 23 14.5	1.2	-23.1	0.8	+14.3	16425.3	7.0	-15.2	-15 395.2	-5725.2	6.6	2.6	+19.3	-8.1
Nov. 3	MT	03 27 50.0	1.0	+169.5	0.1	+15.9	22242.5	7.0	+12.1	+5734.8	-21 490.9	1.8	6.7	+18.4	-7.6
Aug. 10	MU	05 14 56.2	0.8	+744.4	0.1	+79.5	7060.6	11.9	-119.4	+6674.5	-2313.4	11.2	3.9	-86.6	+114.6
Aug. 10	MT	05 17 50.8	1.1	-69.5	0.2	-12.2	15332.2	15.7	-73.9	+14 756.5	-4162.2	15.1	4.3	-74.5	+8.3
Aug. 10	UT	06 17 48.8	1.5	+153.8	0.1	+10.1	8238.7	4.8	+1.1	+8007.7	-1937.3	4.7	1.1	+3.5	+9.6
Aug. 10	MA	06 29 21.8	1.3	+42.6	1.1	-34.9	13717.2	77.8	+69.4	-13 579.7	-1937.3	77.0	11.1	-73.6	+24.8
Aug. 11	MA	06 56 1.9	8.8	-35.3	5.4	+21.7	10906.2	128.9*	-28.7	+9932.9	+4503.7	117.3*	53.5	-35.1	+7.9
Aug. 15	AO	05 06 19.4	3.9	-30.4	0.7	-5.1	17969.8	22.0	+13.2	-17 755.6	-2766.8	21.7	3.4	-13.9	+3.0
Aug. 15	MO	06 57 26.9	0.7	-362.9	0.2	-90.3	21258.5	5.4	-24.2	-20 803.1	-4381.1	5.3	1.1	+5.0	93.5
Aug. 15	AT	07 08 44.6	1.5	-120.2	0.2	-15.6	11311.1	5.7	-7.8	-10617.0	-3901.5	5.3	2.0	+1.9	+17.4
Oct. 18	AT	01 36 32.4	1.6	-49.2	0.1	-4.5	15817.9	7.8	+17.9	+9640.6	-12 540.6	4.7	6.1	+7.3	-16.9
Nov. 13	UT	03 40 33.4	5.8	-160.1	0.3	-8.0	10926.2	6.5	+10.2	+6547.4	-8747.2	3.9	5.2	-0.2	-12.9
July 16	AT	07 10 40.6	19.5	+170.7	12.0*	-104.6	29792.4	193.3*	-6.7	+29 789.4	+417.9	193.2*	12.8	-4.2	-104.9
July 17	MU	08 03 1.4	0.6	-89.5	0.0	-6.4	9535.7	8.3	+108.0	-899.3	+9493.5	0.8	8.3	-3.8	+108.1
July 18	AT	06 54 28.8	1.5	-32.1	0.1	-2.9	16763.8	17.1	-17.1	-1273.8	+16 715.4	1.3	17.1	+4.2	-16.8
Aug. 19	TO	06 08 39.0	26.1	-281.8	0.8	-8.6	8022.1	8.8	+6.8	+7157.1	-3623.5	7.9	4.1	+2.2	-10.7
Sept. 28	MA	03 15 24.7	0.8	+493.9	0.0	+14.6	4341.6	11.0	-73.6	+549.8	-4308.3	1.4	10.9	+5.2	+74.9
Oct. 22	AT	01 15 36.4	0.7	-668.0	0.1	-61.4	17737.8	4.5	-43.2	-1568.8	+17 670.5	0.4	4.5	+64.8	-37.6
mean					0.6	-2.5		14.8	-10.9			12.0	8.2	-6.5	+8.6
s.d.						41.7			46.4					37.4	50.0

*Note:* The four blocks of the table refer to 2015, 2016, 2017 and 2018 events respectively. ‘Sat’ stands for the satellites 1 and 2 in mutual approximation, A = Ariel, U = Umbriel, T = Titania, O = Oberon, M = Miranda.  $t_0$  and  $d_0$  refer to the astrometric topocentric central instant and impact parameter.  $X$  and  $Y$  are the astrometric topocentric inter-satellite ( $\alpha, \delta$ ) distances (cos  $\delta$  applied for  $X$ ) in the sense ‘satellite 1 minus 2’ at  $t_0$ .  $\sigma$  refers to the internal error and  $\Delta$  to the ephemeris offsets of these quantities in the sense ‘observed minus ephemeris’. The ephemeris offset in the central instant is converted from seconds of time ( $\Delta t_0$ ) to mas ( $\Delta t_0, v_0$ ) by using the ephemeris relative velocity  $v_0$  at  $t_0$ . By convention, the relative velocity  $v_0$  is set negative/positive when it points toward/increasing position angle  $\theta$  in equations (1). For the central instant error, the conversion to mas ( $\sigma_{t_0, |v_0|}$ ) is made with the absolute value of  $v_0$ . The JPL DE432 + URA111 ephemerides were used in the comparisons. Time is in UTC. Values marked with ‘\*’ were excluded from the mean and standard deviation computations given at the end (see text).

are translated to  $(X, Y)$  internal relative position errors of 12.0 and 8.2 mas respectively. The mean and standard deviation ephemeris offsets for the central instant were respectively  $-2.5$  and 41.7 mas, and  $-10.9$  and 46.4 mas for the impact parameter. The mean and standard deviation of ephemeris offsets ( $\Delta X, \Delta Y$ ) for the  $(X, Y)$  inter-satellite distances were respectively  $(-6.5$  mas,  $+8.6$  mas) and (37.4 mas, 50.0 mas). Taking all these standard deviations in consideration, and the error contribution from the ephemeris itself, we conservatively estimate that the total external relative position error of our results is 45 mas for each  $(\alpha, \delta)$  coordinate – the same value can be assumed for each of the parallel and orthogonal directions of motion between the satellites. Notice that 12 of the 23 events involve Miranda, the most difficult of the five satellites to measure.

An example of a fitting to an observed apparent relative velocity curve is displayed in Fig. 5, with apparent velocities affected by solar phase angle effects, light deflection, light time, aberration and atmospheric refraction. Plots for the velocity curves of each of the 23 mutual approximations are available as online supporting information.

The relative velocity regime for Uranus’ satellites is quite slow, typically between 0.1 and 0.8 mas  $s^{-1}$ . In contrast, the values for the Jovian moons are one to two orders of magnitude higher, between 1.5 and 7.5 mas  $s^{-1}$ . Even so, we got satisfactory results. The observed relative velocities shown in Table 3 present average internal velocity errors of about 0.02 mas  $s^{-1}$ , or 0.017 mas  $s^{-1}$  for each inter-satellite relative velocity component ( $\dot{X}, \dot{Y}$ ), after discarding a few spurious error values from statistics, as indicated with ‘\*’ in Table 3. The agreement with ephemeris is excellent,

with an average offset of virtually zero mas  $s^{-1}$  and standard deviation of only 0.009 mas  $s^{-1}$  for all 23 mutual approximations. The corresponding  $(\alpha, \delta)$  inter-satellite relative velocity ephemeris offsets ( $\dot{X}, \dot{Y}$ ) are plotted in Fig. 6 for the 23 events indicated in Table 3.

Notice that, by necessity, we must use some planetary ephemeris (the JPL DE432 ephemeris in our case) in the generation of individual ephemeris positions, prior to obtaining relative ephemeris quantities between any two satellites. However, it should be clear that ephemeris distances, relative velocities and inter-satellite  $(X, Y)$  and  $(\dot{X}, \dot{Y})$  components will ultimately depend only upon the used satellite system ephemeris itself, in our case the JPL URA111 ephemeris. This is because the contribution of the planetary ephemeris always cancels out in the computations. Therefore, the ephemeris offsets reported here, in essence, refer to the JPL URA111 ephemeris alone, rather than to any shared contribution from the JPL DE432 ephemeris.

For orbit/ephemeris fitting work, all the 15 873 obtained individual observed distances in mas from the 23 mutual approximations, converted to the astrometric topocentric frame, are freely available in electronic form at the NSDB.<sup>3</sup> We also furnish the individual  $X$  and  $Y$  astrometric topocentric inter-satellite ( $\alpha, \delta$ ) distances in the sense ‘satellite 1 minus 2’ in mas (cos  $\delta$  applied for  $X$ ), derived from the use of the pixel scale and CCD orientation angle computed as described in Section 2.2.

<sup>3</sup><http://nsdb.imcce.fr/nsdb/home.html>

**Table 3.** 23 mutual approximations: results for relative velocity and ( $\dot{X}$ ,  $\dot{Y}$ ) inter-satellite velocities at the central instant.

Date ddmm	Sat 12	$t_0$ UTC (hhmmss.s)	$v_0$ (mas s <sup>-1</sup> )	$\sigma v_0$ (mas s <sup>-1</sup> )	$\Delta v_0 $ (mas s <sup>-1</sup> )	$\dot{X}$ (mas s <sup>-1</sup> )	$\dot{Y}$ (mas s <sup>-1</sup> )	$\sigma(\dot{X}, \dot{Y})$ (mas s <sup>-1</sup> )	$\Delta\dot{X}$ (mas s <sup>-1</sup> )	$\Delta\dot{Y}$ (mas s <sup>-1</sup> )
Oct. 13	MU	01 06 33.7	+0.089	0.023	+0.000	-0.023	-0.086	0.016	-0.000	-0.000
Aug. 23	UT	05 49 34.4	-0.582	0.013	-0.008	+0.114	-0.571	0.009	-0.002	+0.008
Sept. 10	MA	03 55 17.9	-0.833	0.257*	+0.006	-0.254	+0.793	0.182*	-0.002	+0.006
Sept. 10	MT	04 46 10.8	+0.178	0.012	-0.006	-0.122	+0.131	0.008	+0.004	-0.004
Sept. 11	MO	06 15 27.2	+0.139	0.019	-0.012	+0.085	+0.109	0.013	-0.007	-0.009
Sept. 23	AU	03 23 14.5	-0.617	0.023	-0.003	+0.215	-0.578	0.016	-0.001	+0.003
Nov. 3	MT	03 27 5.0	+0.072	0.033	-0.022	-0.069	-0.019	0.023	+0.021	+0.006
Aug. 10	MU	05 14 56.2	+0.102	0.051	-0.006	-0.033	-0.096	0.036	+0.002	+0.005
Aug. 10	MT	05 17 50.8	+0.176	0.051	-0.000	-0.048	-0.170	0.036	+0.000	+0.000
Aug. 10	UT	06 17 48.8	+0.064	0.007	-0.001	-0.015	-0.063	0.005	+0.000	+0.001
Aug. 10	MA	06 29 21.8	-0.808	0.406*	-0.014	+0.114	-0.800	0.287*	-0.002	+0.014
Aug. 11	MA	06 56 1.9	-0.622	2.362*	+0.006	-0.257	+0.566	1.671*	-0.002	+0.005
Aug. 15	AO	05 06 19.4	+0.164	0.052	-0.003	-0.025	+0.162	0.036	+0.000	-0.003
Aug. 15	MO	06 57 26.9	+0.216	0.017	-0.033	-0.044	+0.211	0.012	+0.007	-0.033
Aug. 15	AT	07 08 44.6	+0.132	0.017	+0.002	-0.046	+0.124	0.012	-0.001	+0.002
Oct. 18	AT	01 36 32.4	+0.093	0.013	+0.001	-0.074	-0.057	0.009	-0.000	-0.000
Nov. 13	UT	03 40 33.4	+0.049	0.017	-0.000	-0.039	-0.029	0.012	+0.000	+0.000
July 16	AT	07 10 40.6	-0.604	0.937*	-0.010	-0.014	+0.604	0.663*	+0.000	-0.010
July 17	MU	08 03 1.4	+0.061	0.023	-0.010	+0.061	+0.006	0.016	-0.010	-0.001
July 18	AT	06 54 28.8	+0.086	0.033	-0.003	+0.086	+0.007	0.023	-0.003	-0.000
Aug. 19	TO	06 08 39.0	+0.029	0.016	-0.001	-0.013	-0.026	0.012	+0.001	+0.001
Sept. 28	MA	03 15 24.7	+0.027	0.305*	-0.002	-0.027	+0.003	0.215*	+0.002	-0.000
Oct. 22	AT	01 15 36.4	+0.090	0.016	-0.001	+0.090	+0.008	0.012	-0.001	-0.000
mean				0.024	-0.005			0.017	+0.000	-0.000
s.d.					0.009				0.005	0.009

Note: Table blocks and satellite codes are set as in Table 2.  $t_0$  and  $v_0$  refer to the astrometric topocentric central instant and relative velocity. By convention, the relative velocity  $v_0$  is set negative/positive when it points toward increasing/decreasing position angle  $\theta$  at  $t_0$  in equations (1).  $\dot{X}$  and  $\dot{Y}$  are the astrometric topocentric inter-satellite ( $\alpha$ ,  $\delta$ ) relative velocities ( $\cos \delta$  applied for  $X$ ) in the sense ‘satellite 1 minus 2’ at  $t_0$ .  $\sigma$  and  $\Delta$  refer to relative velocity internal errors and ephemeris offsets in the sense ‘observed minus ephemeris’. The offsets in  $v_0$  were taken from observed and ephemeris absolute values  $|v_0|$ , regardless of the  $v_0$  sign convention in equations (1). The JPL DE432 + URA111 ephemerides were used in the comparisons. Time is in UTC. Values marked with ‘\*’ were excluded from the mean and standard deviation computations given at the end (see text).

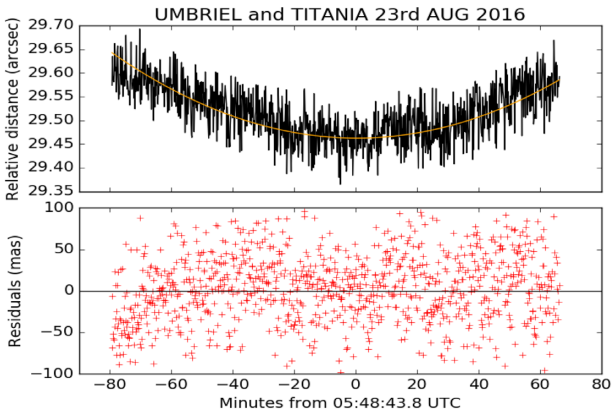


**Figure 2.** Observed sky plane apparent distance curves for Umbriel and Titania in the mutual approximation of 2016 August 23 seen from OPD. Apparent distances are affected by solar phase angle effects, light deflection, light time, aberration and atmospheric refraction.  $t = 0$  is the corresponding observed apparent topocentric central instant. Observed distances are connected in black and the yellow line represents the fitted ones. At the bottom, the red crosses are the residuals of the fitting. We used the computed pixel scale to convert the apparent distances from pixels to arcseconds.

## 7 COMMENTS AND CONCLUSIONS

Until 2040–2050, no probes will be making *in situ* observations of the Uranus system from which one could derive high-quality

astrometric measurements (Hofstadter et al. 2019). Now and for some five years, the planet will be slowly passing through a sky path without many stars. Because of this, no stellar occultations are foreseen in the near future, also preventing us from getting high-quality astrophysical and astrometric data for the moons. Besides, although mutual phenomena deliver high-quality astrometric data, this only occurs every 42 yr at Uranus equinoxes, and the next one will only be in 2050.

Because of the proximity of Miranda, Ariel and Umbriel to the planet’s disc, we must use long-focus telescopes to get a better spatial resolution, resulting in a small FOV of usually a few arcminutes in size, with fewer stars available. Besides, the usual short exposure times needed to avoid light contamination by the planet over the nearby satellites results in underexposed stars. Finally, with the current lack of stars in the sky, we end up with an unevenly distributed insufficient number of reference catalogue stars to map distortions below the 50 mas level, even for a small FOV and using *Gaia*.

In this problematic scenario, a promising alternative for the Uranus system is the astrometric technique of mutual approximations. It accurately and precisely furnishes the central instant at closest apparent approach between two moving satellites in the sky plane. Measurements are made on very small portions of the FOV and thus benefit from the astrometry properties of the *precision premium* – for distances smaller than about 85 arcsec, the effects of astronomical and instrumental distortions largely cancel out, noticing that Uranus’ satellite distances are always smaller than 60

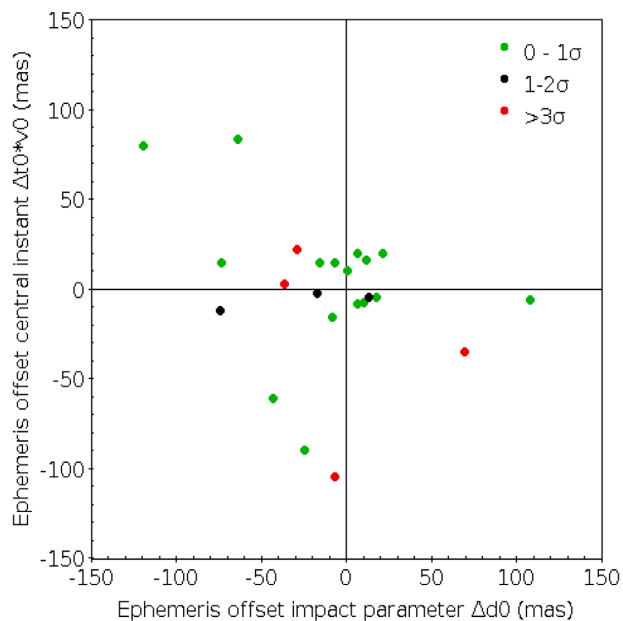


**Figure 3.** Astrometric topocentric ephemeris offsets (mas) for central instant  $t_0$  and impact parameter taken from Table 2 for the 23 mutual approximations. Offsets are in the sense ‘observed minus JPL DE432+URA111 ephemeris’. The colours indicate the total internal error (composed of the individual central instant and impact parameter internal errors) with respect to the  $1\sigma$  internal error of 14.8 mas computed from the central instant and impact parameter internal error averages listed at the bottom of Table 2 (there are no points within  $2-3\sigma$ ).

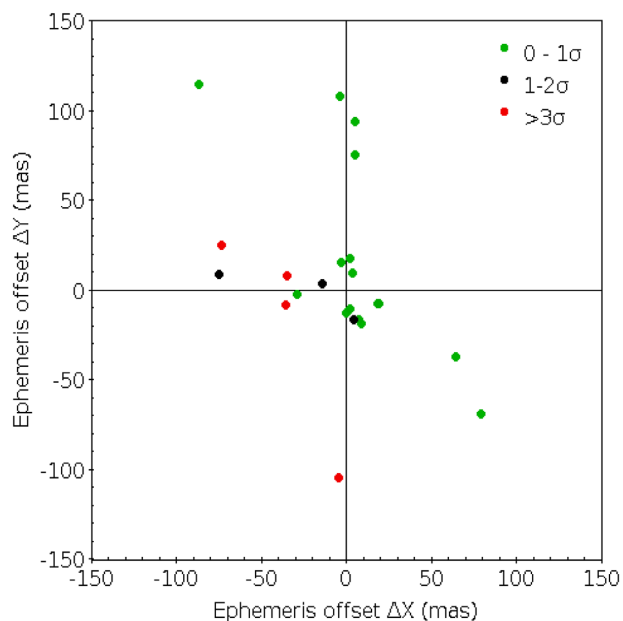


**Figure 4.** Astrometric topocentric ephemeris offsets (mas) for  $X$  and  $Y$  inter-satellite distances ( $\cos \delta$  applied) taken from Table 2 for the 23 mutual approximations. Offsets are in the sense ‘observed minus JPL DE432+URA111 ephemeris’. The colours indicate the total internal error (composed of the individual  $X$  and  $Y$  internal errors) with respect to the  $1\sigma$  internal error of 14.5 mas computed from the  $X$  and  $Y$  internal error averages listed at the bottom of Table 2 (there are no points within  $2-3\sigma$ ).

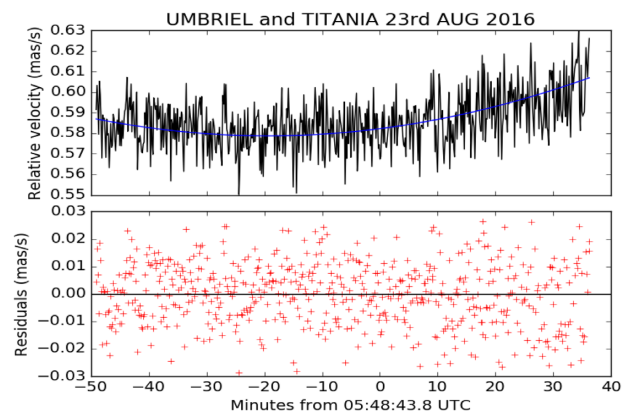


**Figure 5.** Observed sky plane apparent relative velocity curves for Umbriel and Titania in the mutual approximation of 2016 August 23 seen from OPD. Apparent velocities are affected by solar phase angle effects, light deflection, light time, aberration and atmospheric refraction.  $t = 0$  is the corresponding apparent topocentric central instant. Observed relative velocities are connected in black and the blue line represents the fitted ones. At the bottom, the red crosses are the residuals of the fitting. We used the computed pixel scale to convert the apparent relative velocities from pixels  $s^{-1}$  to  $mas s^{-1}$ .

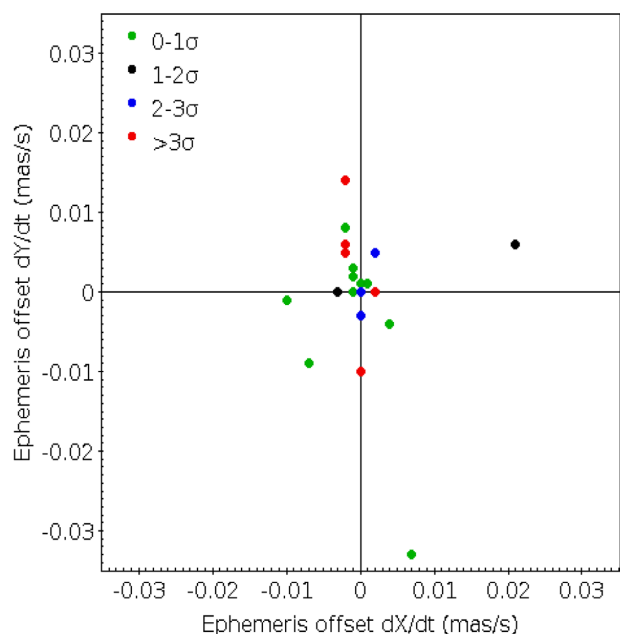


**Figure 6.** Astrometric topocentric ephemeris offsets ( $mas s^{-1}$ ) for  $\dot{X}$  and  $\dot{Y}$  inter-satellite relative velocities ( $\cos \delta$  applied) taken from Table 3 for the 23 mutual approximations. Offsets are in the sense ‘observed minus JPL DE432+URA111 ephemeris’. The colours indicate the total internal error (composed of the individual  $\dot{X}$  and  $\dot{Y}$  internal errors) with respect to the  $1\sigma$  internal error of  $0.024 mas s^{-1}$  computed from the  $\dot{X}$  and  $\dot{Y}$  internal error averages listed at the bottom of Table 3.

arcsec. The central instant is independent of reference star positions and can be directly used in orbital and ephemeris computation work. This technique, inspired by mutual phenomena, is based on the same geometric principles and parameters, and achieves similar precision in central instant as indicated by first applications to the Jovian moons (Morgado et al. 2016, 2019b). Furthermore, an important advantage is that, unlike mutual phenomena, mutual approximations occur virtually at any time outside equinoxes. Another characteristic

is its simplicity. The central instant can be obtained without the need to calibrate or scale the measured instrumental  $(x, y)$  coordinates in pixels. Since the method relies on registering instants, besides relative distances, it is important to accurately record time, but this is also easily done by using GPS receivers or calibrated internet time to 0.1 s precision.

In this context, this paper presents results for 23 mutual approximations involving the five main Uranus satellites: Miranda, Umbriel, Ariel, Titania and Oberon. Observations were made with a 1.6 m aperture Brazilian telescope during 2015–2018. Images were digitally coronagraphed to attenuate the scattered light from Uranus, improving measurements mostly for Miranda, Ariel and Umbriel. We managed to measure the impact parameter in milliarcseconds for the first time, using a variant of the mutual approximations method, developed in this work. This was possible because of the sufficient number of satellites available in the FOV for the Uranus system. We could then derive the pixel scale independently of star catalogues or from the measurements of the involved satellites, by using separate ephemerides and the measured distances of the other nearby satellites in the FOV. In the same way, we could derive relative velocities in  $\text{mas s}^{-1}$  at the central instant  $t_0$ . From the observed central instant and impact parameter, we could also express the results in terms of right ascension and declination  $(X, Y)$  inter-satellite distances in milliarcseconds at  $t_0$  in the ICRS, as well as  $(\dot{X}, \dot{Y})$  relative velocities in  $(\alpha, \delta)$  components at  $t_0$ . The determination of the CCD orientation angle with respect to the  $(\alpha, \delta)$  axes also allowed for computing individual  $(X, Y)$  inter-satellite distances. Although the satellite distances are never larger than 60 arcsec, the pixel scale could be derived with an error of 0.001  $\text{mas pixel}^{-1}$ , and the orientation angle with arcminute precision. A total of 15 873 astrometric topocentric individual relative distances in milliarcseconds were obtained. They are freely available in electronic form at the NSDB. We also gave a guide on how to use our results – central instants, impact parameter, relative distances and velocities, inter-satellite  $(X, Y)$  distances and  $(\dot{X}, \dot{Y})$  relative velocities in  $(\alpha, \delta)$  – as observables in orbital and ephemeris computation work.

From the ephemeris offset analysis in Section 6, by taking the JPL URA111 ephemeris as a reference, we estimated the total external relative positional error of our results in 45 mas for each  $(\alpha, \delta)$  coordinate. The same error of 45 mas can be assumed for each of the directions parallel (in the central instant sense) and orthogonal (in the impact parameter sense) to the motion between the satellites. Notice that 12 out of the 23 mutual events analysed involve Miranda, the most difficult of the five satellites to measure.

The relative velocities for Uranus' main satellites are typically about 0.1–0.8  $\text{mas s}^{-1}$ , a much slower regime when compared to the 1.5–7.5  $\text{mas s}^{-1}$  velocity range for Jovian moons. Even so, for the 23 mutual approximations we obtained an average ephemeris offset of virtually zero  $\text{mas s}^{-1}$  and a standard deviation of 0.009  $\text{mas s}^{-1}$ , indicating that the observed relative velocities are in excellent agreement with the ephemeris.

These error estimates hold for Lainey's ephemeris LA15 (Lainey 2008; Arlot, Birlan & Robert 2016) and for the EM13 ephemeris by Emelyanov & Nikonchuk (2013), because they coincide for all satellites with the JPL URA111 ephemeris within less than 10 mas for the 2015–2018 period of our observations, in accordance with Xie et al. (2019).

For the Uranus system, classical CCD astrometry total errors in relative positions for each coordinate are about 100 mas for Miranda and 50 mas for the other satellites, by taking Oberon as a reference (Camargo et al. 2015). Recently, using a larger

FOV and the *Gaia* DR1 catalogue, Xie et al. (2019) reported observations made between 2014 and 2016, with Miranda–Oberon relative position errors of 44 and 36 mas in  $(\alpha, \delta)$  respectively, and about 20 mas for the other satellite–Oberon pairs, as can be seen in their table 6. This is in agreement with our results. From the ephemeris offsets listed in Table 2, our results including only Miranda (12 events) and not (11) present errors of (35 mas, 47 mas) and (28 mas, 36 mas) in  $(\alpha, \delta)$  respectively. Notice that only four approximations involved Oberon, the satellite with the best ephemeris and that is usually best measured, while it is used as a reference in all the results displayed in table 6 of Xie et al. (2019). These errors start to approach the relative position errors of about 20 mas for mutual phenomena measurements (Assafin et al. 2009; Arlot et al. 2013).

Thus, reinforcing the discussion in Section 2.4 and the conclusions given in Emelyanov (2017), this paper shows the potential of our results and of mutual approximations, in combination with classical astrometry, for improving the current orbits and ephemerides of the main moons of Uranus, with accuracy and precision that could be helpful to future space missions aiming for the system, and for the prediction of future stellar occultations.

## ACKNOWLEDGEMENTS

We thank the anonymous referee for his/her invaluable contribution to improve the paper. We thank T. Bassallo for assisting in some of the observations. This collaboration, as part of the Encelade working group (<http://www.issibern.ch/teams/encelade/>), has been supported by the International Space Sciences Institute (ISSI) in Bern, Switzerland. We are heavily indebted to the authors of the SPICE software toolkit, adapted for use in the PRAIA package. Software routines from the IAU SOFA Collection were used. Copyright ©International Astronomical Union Standards of Fundamental Astronomy (<http://www.iausofa.org>). The work was based on observations made at the Laboratório Nacional de Astrofísica (LNA), Itajubá-MG, Brazil. This study was financed by the Coordenação de Aperfeiçoamento de Pessoal de Nível Superior – Brasil (CAPES) – Finance Code 001. Part of this research was supported by INCT do e-Universo, Brazil (CNPQ grant 465376/2014-2). MA thanks CNPq (Grants 427700/2018-3, 310683/2017-3 and 473002/2013-2) and FAPERJ (Grant E-26/111.488/2013). BM is grateful for the CAPES/Cofecub-394/2016-05 grant. RVM acknowledges the grants CNPq-306885/2013, CAPES/Cofecub-2506/2015, FAPERJ/PAPDRJ-45/2013 and FAPERJ/CNE/05-2015. JIBC acknowledges CNPq grant 308150/2016-3. ARGJ thanks FAPESP proc. 2018/11239-8. GBR acknowledges the support of the CAPES and FAPERJ/PAPDRJ (E26/203.173/2016) grants.

## REFERENCES

- Acton C. H., 1996, *Planet. Space Sci.*, 44, 65
- Arlot J.-E. et al., 1982, *A&A*, 111, 151
- Arlot J.-E. et al., 2013, *A&A*, 557, A4
- Arlot J.-E., Birlan M., Robert V., 2016, *Romanian Astron. J.*, 26, 3
- Assafin M., Campos R. P., Vieira-Martins R., da Silva Neto D. N., Camargo J. I. B., Andrei A. H., 2008, *Planet. Space Sci.*, 56, 1882
- Assafin M., Vieira-Martins R., Braga-Ribas F., Camargo J. I. B., da Silva Neto D. N., Andrei A. H., 2009, *AJ*, 137, 4046
- Assafin M., Camargo J. I. B., Vieira-Martins R., Andrei A. H., Sicardy B., Young L., da Silva Neto D. N., Braga-Ribas F., 2010, *A&A*, 515, A32
- Assafin M., Vieira Martins R., Camargo J. I. B., Andrei A. H., da Silva Neto D. N., Braga-Ribas F., 2011, in Tanga P., Thuillot W., eds, *Gaia Follow-*

- up Network for the Solar System Objects: Gaia FUN-SSO Workshop Proc. IMCCE, Paris, p. 85
- Assafin M., Camargo J. I. B., Vieira-Martins R., Braga-Ribas F., Sicardy B., Andrei A. H., da Silva Neto D. N., 2012, *A&A*, 541, A142
- Astropy Collaboration, Robitaille T. P., Tollerud E. J. Astropy Collaboration et al., 2013, *A&A*, 558, A33
- Benedetti-Rossi G., Vieira-Martins R., Camargo J. I. B., Assafin M., Braga-Ribas F., 2014, *A&A*, 570, A86
- Butcher E., Stevens R., 1981, Newsletter Kitt Peak Natl. Observ., 16, 6
- Camargo J. I. B. et al., 2014, *A&A*, 561, A37
- Camargo J. I. B. et al., 2015, *A&A*, 582, A8
- Charnoz S. et al., 2011, *Icarus*, 216, 535
- Crida A., Charnoz S., 2012, *Science*, 338, 1196
- Desmars J. et al., 2015, *A&A*, 584, A96
- Dias-Oliveira A. et al., 2013, *MNRAS*, 432, 225
- Emelyanov N. V., 2017, *MNRAS*, 469, 4889
- Emelyanov N. V., Nikonchuk D. V., 2013, *MNRAS*, 436, 3668
- Gomes-Júnior A. R. et al., 2015, *A&A*, 580, A76
- Gomes-Júnior A. R., Assafin M., Beauvalet L., Desmars J., Vieira-Martins R., Camargo J. I. B., Morgado B. E., Braga-Ribas F., 2016, *MNRAS*, 462, 1351
- Hestroffer D., 1998, *A&A*, 336, 776
- Hidas M. G., Christou A. A., Brown T. M., 2008, *MNRAS*, 384, L38
- Hofstadter M. et al., 2019, *Planet. Space Sci.*, 177, in press
- IAU SOFA Board, 2018, IAU SOFA Software Collection, Issue 2018-01-30. <http://www.iausofa.org>
- ItJacobson R. A., 2014, *AJ*, 148, 76
- Lainey V., 2008, *Planet. Space Sci.*, 56, 1766
- Lainey V., Duriez L., Vienne A., 2004a, *A&A*, 420, 1171
- Lainey V., Arlot J.-E., Vienne A., 2004b, *A&A*, 427, 371
- Lainey V., Arlot J. -E., Karatekin O., Van Van Hoolst T., 2009, *Nature*, 459, 957
- Lindgren L., 1977, *A&A*, 57, 55
- Morgado B. et al., 2019a, *A&A*, 626, L4
- Morgado B. et al., 2019b, *MNRAS*, 482, 5190
- Morgado B., Assafin M., Vieira-Martins R., Camargo J. I. B., Dias-Oliveira A., Gomes-Júnior A. R., 2016, *MNRAS*, 460, 4086
- Nogueira E., Brassier R., Gomes R., 2011, *Icarus*, 214, 113
- Peng Q. Y., Vienne A., Lainey V., Noyelles B., 2008, *Planet. Space Sci.*, 419, 1977
- Peng Q. Y., He F., Lainey V., Vienne A., 2012a, *MNRAS*, 56, 1807
- Peng Q. Y., Vienne A., Zhang Q. F., Desmars J., Yang C. Y., He H. F., 2012b, *AJ*, 144, 170
- Sicardy B. et al., 2006a, *J. Geophysical Res.*, 111, S91
- Sicardy B. et al., 2006b, *Nature*, 439, 52
- Smith B. A. et al., 1986, *Science*, 233, 43
- Thomas P. C., 1988, *Icarus*, 73, 427
- Vienne A., Thuillot W., Arlot J.-E., 2001, in Note Sci. et Tech. de l'I.M.C.C.E. p.S077
- Widemann T. et al., 2009, *Icarus*, 199, 458
- Xie H. J., Peng Q. Y., Wang N., Vienne A., Li C. W., Xie M. N., Liu Z. W., 2019, *Planet. Space Sci.*, 165, 110

## SUPPORTING INFORMATION

Supplementary data are available at *MNRAS* online.

Please note: Oxford University Press is not responsible for the content or functionality of any supporting materials supplied by the authors. Any queries (other than missing material) should be directed to the corresponding author for the article.

This paper has been typeset from a  $\text{\TeX}/\text{\LaTeX}$  file prepared by the author.